Design, Modeling, and Analysis of a Liquid Cooled Proprioceptive Actuator for Legged Robots

Taoyuanmin Zhu, Joshua Hooks, and Dennis Hong[1]

***Abstract*— Thermal management has always been an essential part of designing robots for extended run times in real world scenarios. Recently, legged robots that utilize proprioceptive actuators have shown impressive results in a laboratory setting, but in order for them to be successful in the real world, it is necessary to manage the excessive joule heating produced by the actuators. To address this need, this paper presents a new high performance proprioceptive actuator with liquid cooling designed for dynamic legged robots. Prior work in the area of liquid cooled actuators fails to address how a liquid cooling system would affect the performance of a legged robotic system as a whole. This work develops a new thermal model that is capable of modeling multiple liquid cooled actuators within a single cooling system. Using this new model as a design tool we were able to determine the trades-offs between peak torque and continuous torque resulting from varying cooling systems.**

I. INTRODUCTION

In recent years, the legged robotics community has begun to move away from stiff, high accuracy position controlled actuators often found in manufacturing and automation. Traditionally, these stiff and rigid actuators worked well in manufacturing because the operating environment is known and disturbances are relatively small. However, this is not the case for legged robotics where it has been shown that an impedance control strategy is advantageous compared to that of a rigid position control strategy [1].

Proprioceptive actuators are one of the technologies being used to provide the needed compliance for successful legged robotic locomotion. Proprioceptive actuators consist of high torque electric motors (motors with a large air gap radius) combined with a small gear reduction or no gear reduction. The benefits of direct drive actuators (no gear reduction) are discussed in [2], explaining that transmission transparency leads to proprioceptive force sensing, impact mitigation, and high bandwidth control. In conjunction with this work Kim et al. demonstrates in [3] and [4] how a low gear reduction both preserves the transparency of the transmission and provides increased torque amplification compared to that of a direct drive actuator. The legged robots in [5], [6],[7], [8], [9] show that robots designed with proprioceptive actuators are capable of extremely dynamic locomotion including running and jumping.

Additionally, proprioceptive actuators are making the natural extension into the prosthesis community where in [10], the authors present a knee and ankle that utilize proprioceptive actuators. These actuators are even proving beneficial for sim-to-real applications due to the simplicity of modeling their dynamics which helps to close the reality gap [11].

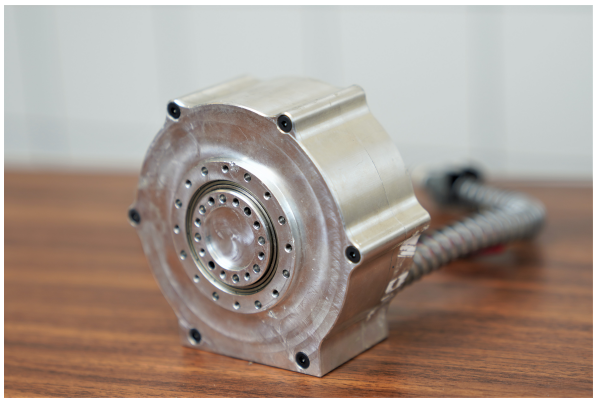

Fig. 1: BEAR module

One of the major draw backs of proprioceptive actuators is their susceptibility to overheating due to excessive Joule heating [12]. Joule heating is the heat produced from an electrical current going through the windings of a motor. Proprioceptive actuators require large currents in order to produce the required torques for legged locomotion, resulting in excessive amounts of Joule heating. Without an efficient way of dissipating the excess heat from the actuators these types of robots will only be able to run for a short amount of time, very much putting into question their use in practical real-world applications. Thermal management for electric motors is a mature field, however many of the techniques used require the addition of large and heavy cooling systems. Unfortunately, in legged robotics mass and volume are at a premium and the addition of a heavy cooling system could actually result in a degradation of heat dissipation due to the increased torque required to account for the mass of the cooling system.

For this reason the thermal management for a legged robotic system must be designed intelligently [13]. In [14] the authors show that large improvements in heat dissipation can be achieved by connecting the stator of the motor directly to the motor housing and designing the housing to act as a heat sink. Multiple studies [14], [15], [16], [17] have shown that liquid cooling can vastly improve the heat dissipation of a single actuator. Unfortunately, all of the previous studies only analyze a single liquid cooled actuator and do not consider the consequences of liquid cooling for the entire

*This work was supported by the ONR through grant N00014-15-1-2064.

[1]All authors are with the Robotics and Mechanisms Laboratory (RoMeLa) at the University of California, Los Angeles (UCLA), Los Angeles, CA 90095, USA. {tymzhu, hooksj, dennishong}@ucla.edu

Manuscript 318 submitted to IEEE/ASME International Conference on Advanced Intelligent Mechatronics. Received March 7, 2019.

robotic system.

To address the major drawback of overheating in proprioceptive actuators we introduce the Back-Drivable Electromechanical Actuator for Robotics (BEAR) with liquid cooling. BEAR is a proprioceptive actuator specifically designed for dynamic legged robotics (Fig. 1). This actuator consists of a commercial off the shelf brushless DC (BLDC) motor with a single stage planetary gearbox. The actuator's motor housing design and stator connection were optimized for increased heat dissipation in conjunction with a liquid cooling system to allow for continuous use of the actuator. The overall specs of the BEAR are summarized in Table I. In addition, we present a thermal model that builds off of the previous works to better represent the heat dissipation of a liquid cooled robot. Finally, we show that our newly developed model can be used as a tool for choosing the proper cooling system for a given legged robot.

TABLE I: BEAR Specs

Mass (g)	670
Gear Reduction	10:1
Voltage (V)	30
Max Current (A)	60
Peak Torque (Nm)	32
Cont. Torque (air cooled, Nm)	7.8
Cont. Torque (liquid cooled, Nm)[1]	~21
Max Velocity (rpm)	300

II. BEAR DESIGN

A. Mechanical Design

The BEAR was designed to provide the torque and speed required for a legged robotic platform to perform dynamic locomotion tasks without sacrificing the transmission transparency required for proprioceptive force control and impact mitigation. For this reason, the BEAR is built with an efficient single stage planetary gearbox and a large air gap radius motor with superior torque density characteristics.

1) Rotor and Stator Design: As in [6] and [2], the BEAR's internal BLDC motor was selected to optimize torque density: the ratio of the motor's peak torque capability to it's mass. Most commercially available actuators focus on optimizing the overall power density: the ratio between the motor's overall mechanical power and it's mass. The peak power output will occur at a relatively high rpm and output torque. As Kim et al. points out in [3] this metric is not useful for legged robotics applications where large torques are required from the actuator at low motor velocities. Thus, the primary metric to consider for legged robotic actuators is the torque density. The following relations were used to analyze a motor's torque density potential [18]:

$$\tau \propto r_g^2 \tag{1}$$
$$\tau \propto l \tag{2}$$
$$M \propto r_g \tag{3}$$
$$M \propto l \tag{4}$$

Where, r_g is the air gap radius of the motor, l is the axial length of the stator, M is the mass of the motor, and τ is the torque. From (1) and (3) it is clear that a larger air gap radius will lead to higher torque densities because of the quadratic relationship whereas from (2) and (4) it is evident that increasing the axial length will have no affect on the torque density of the motor. Similar to the results in [2] we found that the U8 motor from T-Motor was the best commercially available motor for our application.

2) Gearbox Design: Most actuator designs have a large gear reduction in order to increase their torque density. However, large gear reduction compromises the 'transparency' of the transmission which is critical for high speed impedance control [2], [3]. Increasing the transparency of the system requires reducing the dynamics of the gearbox - i.e. reflected inertia, friction, and backlash. A single stage planetary gearbox with 10:1 gear reduction was chosen.

The benefits of having a gearbox with low reflected inertia and friction is most readily seen in Fig. 3. The top plot in Fig. 3 shows the torque curve for a Dynamixel MX-106 actuator, a commercially available actuator with a gear reduction of 225:1. When the MX-106 is driven forward the dynamics behave as expected; The torque is the product of the motor constant and current. However, when the MX-106 is back-driven this relation breaks down. The torque becomes a highly non-linear function leading to the failure of the gearbox before max current could be supplied to the actuator. On the other hand, the bottom plot in Fig. 3 shows that the BEAR always behaves as expected. The difference in the two curves in Fig. 3 (b) is due to small friction losses in the gearbox and the motor hysteresis torque. The back-drivability of the BEAR has two significant benefits. First, the gearbox will not break due to large impact forces. Second,

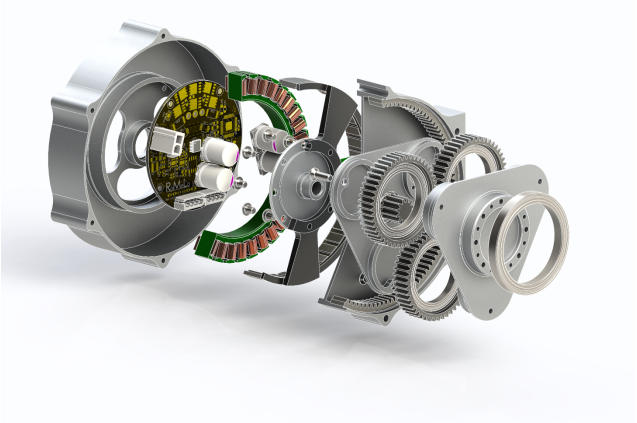

Fig. 2: BEAR module exploded view of mechanical design.

[1]Varies depending on the cooling system

Manuscript 318 submitted to IEEE/ASME International Conference on Advanced Intelligent Mechatronics. Received March 7, 2019.

the actuator is capable of performing proprioceptive force sensing. This implies that without the addition of external sensors the actuator is able to detect external disturbances that are larger than the difference between the two torque curves in Fig. 3 (b).

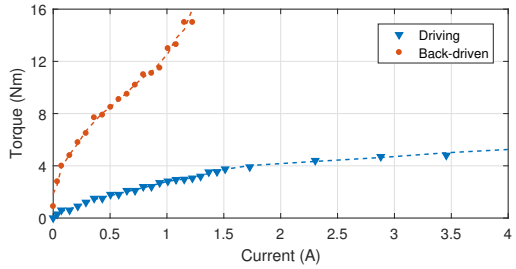

(a) Torque curve for high reduction MX-106 actuator

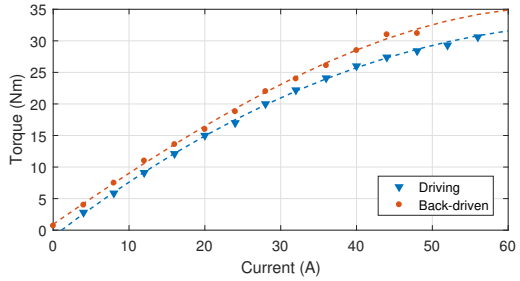

(b) Torque curve for BEAR

Fig. 3: Comparing stall torque curves for high gear reduction gearboxes vs low gear reduction gearboxes.

3) Housing Design: The housing is comprised of three aluminum pieces. The top cap seals the gearbox and secures the output shaft, the middle section houses the planetary gearbox, and the bottom section houses the electric motor and electronics. In addition to housing the electric motor, the bottom section is also carefully designed to act as a heat sink for the motor stator. As shown in Fig. 4, the stator winding of the motor is connected to the motor housing via thermal interface material (Bergquist Gap Filler 4000). During assembly of a BEAR, gap filler is injected in-between each stator spoke, completely filling the gap and making a direct connection to the aluminum housing underneath. This method ensures that heat dissipation occurs via conduction rather than convection, reducing the thermal resistance between the stator winding and the motor housing. Further discussion is in Section III.

To further strengthen the heat dissipation properties of the bottom section, the face directly opposite the stator is designed with liquid cooling channels. The channels act like heat fins, decreasing the overall thermal resistance of the housing. The aluminum channels are sealed via a polycarbonate plate with quick disconnect ports acting as the inlet and outlet for the liquid coolant.

B. Electrical Design

The BEAR is built with an on board motor driver and controller that uses a Multidrop bus (MDB) and RS-485

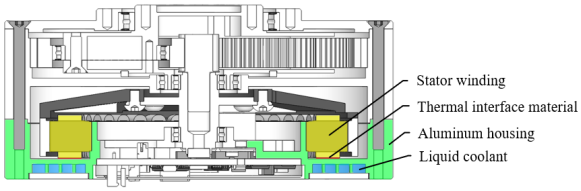

(a) Cross section view

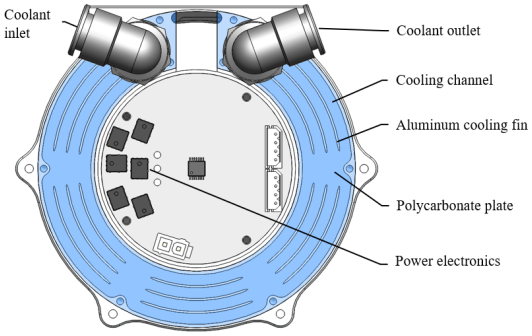

(b) Back view

Fig. 4: Liquid cooling design

communication allowing for multiple actuators to be daisy chained together. This all-in-one design is similar to the architecture found in dynamixel actuators (Robotis Inc.). The electrical system is centered around the MCU (STM32F446, STMicroelectronics), running at 180MHz. The MCU sends PWM signal to a 3-phase motor pre-driver (DRV8305, Texas Instruments). Rotor position feedback is provided by an on-axis 14-bit magnetic absolute encoder (AS5047P, AMS). Additionally, the MCU monitors the temperature levels of the system through a digital temperature sensor that is on the PCB and a thermocouple that is connected directly to the motor windings. High-level position, torque, or velocity commands are sent to the MCU using a custom RS-485 protocol at 8Mbps.

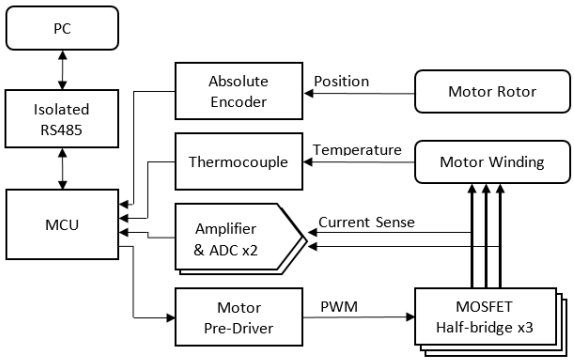

Fig. 5: High level electrical design overview.

C. CONTROL STRUCTURE

The underlying control structure relies on a 22 kHz Field Oriented Control (FOC) [19] [20]. This control loop

accurately controls the current that is being driven through the windings at any given time using a PI loop. There are two control loops that feed into the FOC controller; the first is a generic PID controller that can control position, velocity, or force. The second loop uses a feed-forward compensator to remove the effects of the cogging torque.

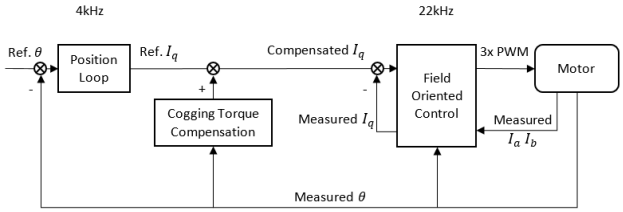

Fig. 6: High level block diagram of control structure.

1) Cogging Torque Compensation: Cogging torque is primarily caused by the interaction between the permanent magnets and the stator core. This relationship causes torque ripples, shown by the blue curve in Fig. 7, that can cause inaccuracies in force control and jerky motion at low speeds. The cogging torque compensator developed in this paper is similar to the one presented in [21]. Cogging torque is a function of position, which can be mapped a-priori through a look up table. The compensator is a feed forward term that looks up the known cogging torque given the current position and commands the inverse to cancel out the effects of the cogging torque. Fig. 7 shows that the compensator was able to decrease the cogging torque ripple by a factor of 10.

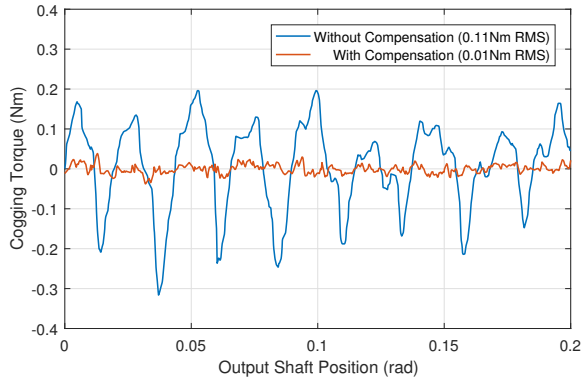

Fig. 7: Comparing the uncompensated BEAR cogging torque to the compensated BEAR cogging torque.

III. Thermal Model

The main source of heat generation in an electric actuator is from Joule heating or Ohmic loss. Ohmic loss (P_e) is a function of the current (I) and the resistance of the windings (R_e).

$$P_e = R_e I^2 \tag{5}$$

The resistance in the windings is a function of the temperature of the windings themselves.

$$R_e = R_o[1 + \alpha(T_w - t_o)] \tag{6}$$

Where R_o is the nominal resistance of the windings at the nominal temperature T_o, T_w is the current temperature of the windings, and α is the temperature coefficient for the windings material which is $0.0039\Omega/K$ in this case for copper. A commonly used lumped mass thermal model for an air cooled electric actuator is shown in Fig. 8 [17] [15] [22].

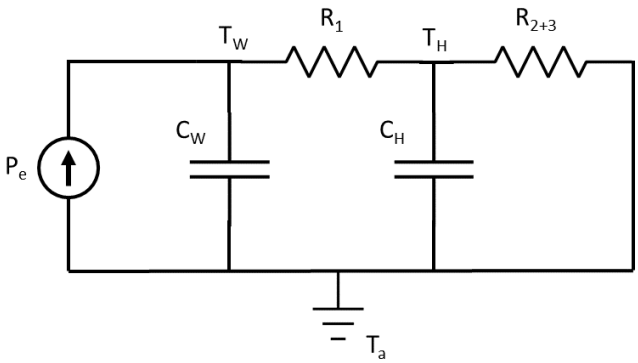

Fig. 8: A simple lumped mass thermal model of an electric actuator.

For this simple model T_w is the temperature of the windings, C_w is the thermal capacitance of the windings, R_1 is the windings-to-housing thermal resistance, T_H is the temperature of the housing, C_H is the thermal capacitance of the housing, R_{2+3} is the housing-to-ambient thermal resistance, and T_a is the ambient air temperature. This simple model has been shown to accurately model an air cooled electric actuator. [17] and [15] both used this simple model to model a liquid cooled electric actuator, making the assumption that the cooling liquid remained at a constant temperature with infinite thermal capacitance. This is a reasonable assumption when testing a single actuator, however this is not the case for a robot that is comprised of multiple liquid cooled actuators. For a more accurate model an additional RC circuit must be added in series to represent the thermodynamics of the liquid and radiator.

In [14] the authors discuss the multiple paths in which heat can dissipate from the housing of an actuator. Specifically they highlight the differences between areas of the housing that dissipates heat through conduction and areas where heat is dissipated through convection. Similar to their work much of the heat will be dissipated by conduction from the area that is in contact with the cooling liquid, however some heat will also dissipate directly from the housing to the ambient air through convection. From these additions we developed the thermal model shown in Fig. 9, for our liquid cooled electric actuators.

Where R_4 is the thermal resistance between the housing and the liquid, R_5 is the thermal resistance of the radiator, and C_L is the thermal capacitance of the cooling liquid. The model also introduces a voltage divider on the

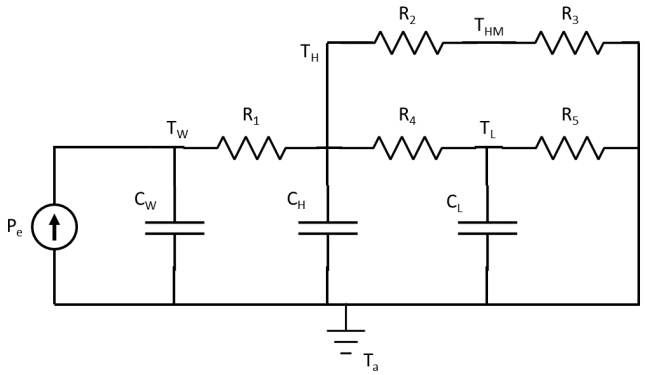

Fig. 9: A lumped mass model that includes the thermal properties of the liquid cooling system.

branch between the housing temperature and the ambient air temperature. The voltage divider represents the difference between the actual temperature of the housing (T_H) and the measured temperature (T_{HM}). The difference in temperature is the result of the thermocouple being attached to the side of the housing during testing. The model shown in Fig. 9 produces the following differential equations describing the thermodynamics of the system.

$$\frac{dT_W}{dt} = \frac{1}{C_W}\left[P_e - \frac{T_W - T_H}{R_1}\right] \tag{7}$$

$$\frac{dT_H}{dt} = \frac{1}{C_H}\left[\frac{T_W - T_H}{R_1} - \frac{T_H - T_L}{R_4} - \frac{T_H - T_a}{R_2 + R_3}\right] \tag{8}$$

$$\frac{dT_L}{dt} = \frac{1}{C_L}\left[\frac{T_H - T_L}{R_4} - \frac{T_L - T_a}{R_5}\right] \tag{9}$$

$$T_{HM} = T_H - \frac{R_2(T_H - T_a)}{R_2 + R_3} \tag{10}$$

This new model is now capable of representing a liquid cooling system with multiple actuators. Assuming that the liquid temperature is the same throughout the system then each actuator model can be connected in parallel. This will result in exactly the same model as Fig. 9 except that now if N actuators are in the system P_e, C_W, and C_H are scaled by N and R_1, R_2, R_3, and R_4 are scaled by $1/N$. The thermal capacitance of the liquid (C_L) will increase depending on how much liquid is added to fill the entire system and R_5 will remain unchanged since this is only dependant on the efficiency of the radiator and pump being used.

A. Parameter Estimation

A number of experiments were run in order to both model and analyze the BEAR actuators thermal properties. The data collected from each experiment included: current in the windings, winding temperature, housing temperature, cooling liquid temperature, and ambient air temperature. The current and temperature of the windings was collected via the actuators motor controller and all other temperatures were collected from additional thermocouples. Each one of the experiments started at room temperature and were allowed to go until the system reached steady state or 90 °C. In order to apply the correct amperage to all three windings a large current was applied to the direct axis current (i_d) and a small current was applied to the quadrature current (i_q), with the magnitude of the sum of the two vectors equaling to the desired current. The i_q was used to slightly oscillate the actuator causing the i_q and i_d to change between phases. This ensured that all three winding phases heated up evenly, rather than locking the motor and only using i_d which would result in more current being applied to only one of the phases.

Three table top experiments were performed to estimate the model described in Fig. 9: air cooling with 8 amps being supplied to the windings, liquid cooling with 20 amps being supplied to the windings, and liquid cooling with 30 amps being supplied to the windings. Simulink's parameter estimation tool was used to estimate the model parameters. All three experiments were used simultaneously during the estimation process to find a unified set of parameters that worked for all three experiments.

The first set of liquid cooling experiments used a single 120mm fan radiator (EKWB EK-AluStream SE 120 + EK-ACR SPC-60 PWM) which will be referred to as radiator I. Another radiator that used a dual 120mm fan radiator (EKWB EK-CoolStream SE 240 + EK-XRES 100 DDC 3.2 PWM Elite), which will be referred to as radiator II, was also used throughout testing. To identify radiator II, another experiment was run using 30 amps in the windings. Changing the radiator only affects R_4, R_5, and C_L and for this reason only these values were allowed to be changed during the parameter identification process. Table II provides a summary of the estimated values, where all thermal resistances are in K/W and thermal capacitences are in J/K.

TABLE II: Summary of Estimated Parameters

	Air	**Radiator I**	**Radiator II**
R_1	0.219	0.219	0.219
R_2	0.177	0.177	0.177
R_3	3.822	3.822	3.822
R_4	-	0.012	0.006
R_5	-	0.071	0.039
C_W	63.64	63.64	63.64
C_H	274.8	274.8	274.8
C_L	-	2214	3302

IV. Experiment Results

A number of experiments were performed to analyze BEAR's liquid cooling capabilities and to confirm that the derived model could accurately predict the thermodynamics of a complete robotic system. In addition to the experiments used to estimate the model parameters in the previous section three more table top tests were run: 25 amps with radiator I, 30 amps with radiator II (this test was used to estimate the radiator II parameters), and 35 amps with radiator II.

The next series of tests were run on a complete robotic system. The Non-Anthropomorphic Biped: Version 2 (NABi-V2) robotic platform is a legged robotic platform built with

Manuscript 318 submitted to IEEE/ASME International Conference on Advanced Intelligent Mechatronics. Received March 7, 2019.

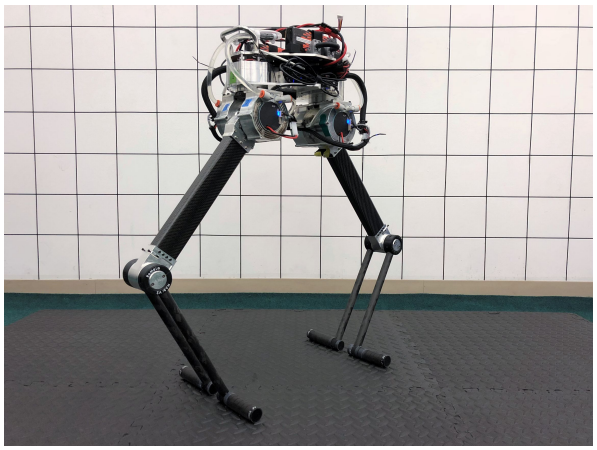

Fig. 10: Non-Anthropomorphic Biped: Version 2 (NABi-V2) robotic platform

6 BEAR modules [23]. In two experiments, one at 20 amps and one at 30 amps, four of NABi-V2's BEAR's were liquid cooled using radiator I. It was found that our model could successfully predict the thermodynamics for a full robotic system, which is most readily seen by the comparison of the table top test and the NABi-V2 test at 30 amps in Fig. 11.

In the first plot of Fig. 11 the system reaches a steady state winding temperature of 74°C, which will not cause the actuator to overheat. The simple model in Fig. 8 predicts no change between the table top test of a single actuator and that of a system with multiple actuators because it uses the assumption that the radiator is perfect and that the liquid temperature never increases. However, this is not what occurs in reality as shown by the second plot in Fig. 11 which shows that the system would have overheated if the experiment had been allowed to continue. Our newly developed model predicts both if the system will overheat and when the system will overheat. A summary of all experiments, showing the RMS error values between the model's predicted temperature and the measured temperature is presented in Table III[2].

TABLE III: RMS errors for experiments

	$T_W(K)$	$T_H(K)$	$T_L(K)$
*8 amps Air	0.258	0.222	-
*20 amps rad I	0.233	0.249	0.157
25 amps rad I	0.546	0.793	0.666
*30 amps rad I	0.426	0.233	0.238
30 amps rad II	1.924	0.522	0.152
35 amps rad II	2.176	0.215	0.752
20 amps NABi-V2	1.622	0.557	2.273
30 amps NABi-V2	3.394	0.906	0.666

V. Liquid Cooling Design Discussion

A. Optimizing Continuous Torque

Using the identified model and the comparison between the two different radiators we were able to look at the optimal cooling system for a given robot using a specific

[2]Experiments with a * were used to estimate parameters.

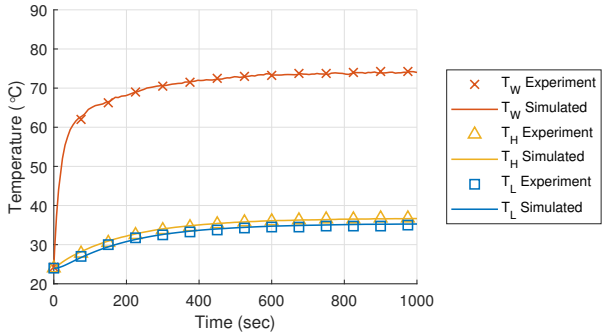

(a) single actuator test at 30 amps using radiator I

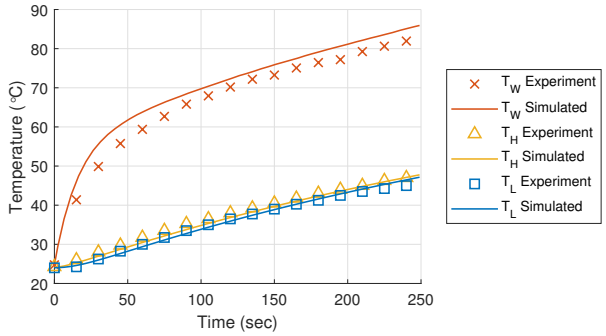

(b) NABi-V2 robotic platform test at 30 amps using radiator I

Fig. 11: Experimental and simulation results for single actuator and NABi-V2 robotic platform

actuator. In our experiments radiator I weighed 1.06 kg and radiator II weighed 2.20 kg, and from the estimated values the thermal resistance of R_4 and R_5 dropped by half from radiator I to II. From these two data point we assumed that the relationship between a cooling systems mass and it's thermal resistances were linear. Although this is most likely an incorrect assumption as there are many factors that play into a cooling system (cooling liquid, pump type, radiator type, line gauge, etc...), this assumption provides useful insight when looking at the design of a robot's liquid cooling system. The continuous torque density of an actuator is the ratio between an actuator's continuous torque and it's mass. Here we are defining the continuous torque density as the ratio between the actuator's continuous torque and the actuators "effective" mass, where the effective mass is the mass of the actuator plus the mass of the cooling system divided by the number of actuators on the robot (we are only including the actuators that would be used to support the robot). Fig. 12 shows the effective continuous torque density as a function of the number of actuators on a robotic system for a given actuator and cooling system.

This analysis reveals that for a given robot there is an optimal cooling system that will maximize the actuator's continuous torque capabilities. The optimal point equates to a cooling system that can fully account for the heat generated by the actuators. Whereas, if the cooling system is too small the liquid will heat up, reducing the effectiveness of the system. If the cooling system is too large the system

returns marginal gains in terms of heat dissipation compared to the additional mass. The green dashed line is the baseline continuous torque of the BEAR with air cooling, and we can see that any practical cooling system will greatly improve the continuous torque density of the system. The red line corresponds to radiator I and the yellow line corresponds to radiator II from the above experiments.

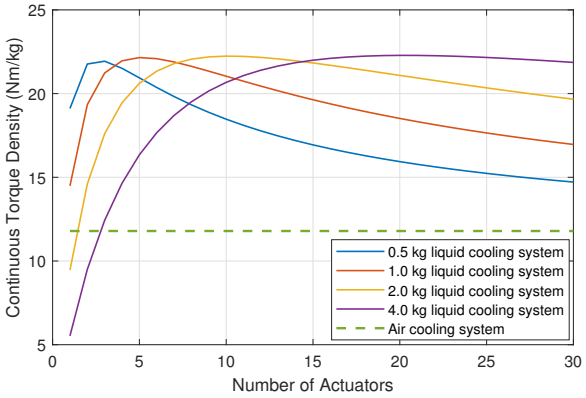

Fig. 12: Continuous torque density compared to the number of load bearing actuators on the robot.

B. How actuator design affects cooling system design

Another way of analyzing the design of the cooling system is by looking at the continuous torque density compared to the effective mass of the actuator (Fig. 13). The solid line, representing the BEAR module, shows that ~25% of the effective mass should go to the cooling system in order to maximize the continuous torque density. The point plotted on the solid line corresponds to the NABi-V2 experiment with radiator I.

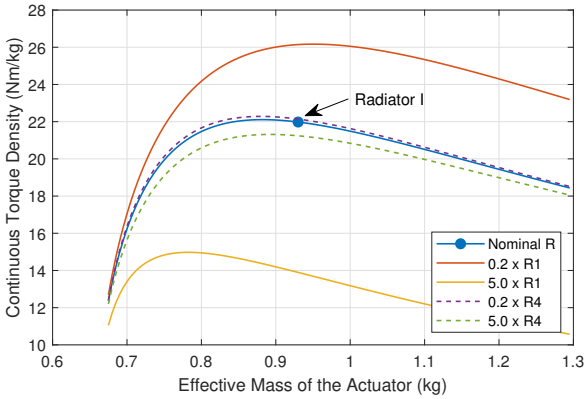

Fig. 13: Continuous torque density compared to the effective mass of the actuator.

Fig. 13 also gives us insight into how actuator design effects the design of the liquid cooling system. The solid red and yellow curves represent R_1 being scaled by 0.2 and 5 respectively. Scaling R_1 effectively scales how well the windings transfer heat to the housing and how this affects the cooling systems design. Fig. 13 unsurprisingly reveals that R_1 limits the overall actuator performance, and if R_1 is large, it will be impossible to effectively cool the windings regardless of the cooling system. However, if R_1 is small, we continue getting benefits from better cooling systems. This is a major reason that the BEAR was designed with conductive cooling for the windings and why we see an order of magnitude difference in R_1 between the BEAR and the Maxon that had a retrofitted cooling system in [17].

The dashed lines in Fig. 13 demonstrate what happens if R_4 is varied, i.e. changing the aluminum fin design on the housing of BEAR. This analysis shows that minimal benefits can be gained from optimizing the fin design of the BEAR housing, because the thermal resistance is all ready small.

C. Choosing a cooling system from design specifications

Up until now we have only considered how liquid cooling affects the continuous torque of the actuators on a robotic system, however peak torque is another critical parameter for a legged robot. When designing a legged robot continuous torque density can be designed for by determining nominal tasks that the robot should be capable of performing. For example, the robot should be able to travel at a certain velocity indefinitely. The required peak torque density is typically more difficult to be designed for, but is often determined with respect to the desired disturbance rejection capabilities of the robot. Essentially, the difference between an actuator's peak torque and nominal operation torque is the amount of force reserved for disturbance rejection.

To look at both peak torque and continuous torque we measured the duration of time the actuator could stay at a constant torque until the system overheated for a given cooling system, Fig. 14. Once again we used the effective mass of the actuator to calculate torque density in order to be able to fairly compare the different cooling systems. The starting points of the curve represent the peak torques and the end points represent the continuous torques. As we saw from Fig. 12 and Fig. 13 if we choose the cooling system that optimizes the continuous torque of the system we see a 100% increase in the continuous torque density of the system, however we also see a 30% decrease in peak torque density. An interesting result is observed when utilizing a cooling system that is undersized. The yellow curve represents a cooling system that uses radiator I with 20 BEAR modules, and it still shows a large gain in continuous torque density of 65%, but now the peak torque density only decreases by 6%.

From this analysis we believe that undersized cooling systems should be considered when designing a legged robot. The authors of this paper are now considering using smaller tube diameters and a smaller reservoir to reduce the overall amount of liquid in the system. The proposed redesign would restrict the flow of the liquid and may require a higher pressure pump. These changes may have drastic effects on the thermal properties of the cooling system and further work needs to be done. It should also be noted that liquid cooling systems add complexity to the mechanical design of a robot.

In the development of NABi we experienced many leaks and tube routing issues. Depending on the robot and the performance requirements the added complexity may not be worth the performance increase. Lastly, we would also like to say that all results in this paper are from a single robotic platform and actuator type and more work is required to verify that our findings extend to different robots and different actuators.

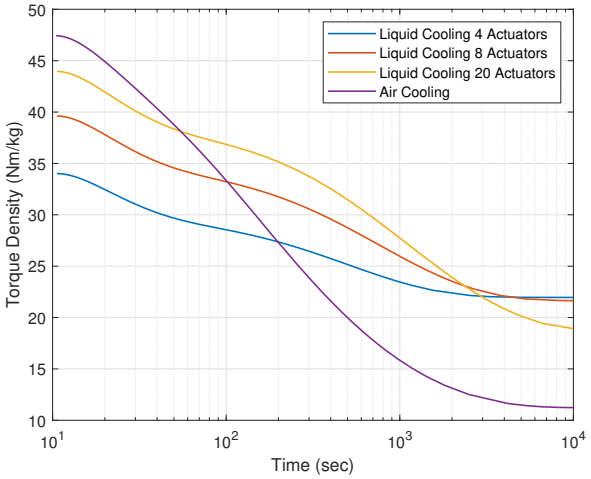

Fig. 14: How long the actuator is able to maintain a certain torque density before overheating, using radiator I and BEAR actuators.

VI. CONCLUSIONS

Proprioceptive actuators have shown that they can provide legged robots with the speed and power required for dynamic locomotion in unstructured environments. However, due to the required electrical current of these actuators, the question remains are they viable for real-world tasks requiring extend run times. This paper tries to take a step in answering that question by presenting the liquid cooled BEAR. In this paper, we have shown that a liquid cooling system provides large improvements in the continuous torque of the actuator, helping to extend the run time of the robot. With the newly developed modeling techniques we are hoping to continue developing liquid cooling systems that are specifically designed for a given robotic system.

ACKNOWLEDGMENT

This work was supported by the ONR through grant N00014-15-1-2064.

REFERENCES

[1] M. H. Raibert, B. H. Brown, and M. Chepponis, "Experiments in balance with 3d one-legged hopping machine," *The International Journal of Robotics Research*, vol. 3, pp. 75–92, 1984.

[2] G. Kenneally, A. De, and D. E. Koditschek, "Design principles for a family of direct-drive legged robots," *IEEE Robotics and Automation Letters*, vol. 1, no. 2, pp. 900–907, 2016.

[3] S. Seok, A. Wang, D. Otten, and S. Kim, "Actuator design for high force proprioceptive control in fast legged locomotion," in *2012 IEEE/RSJ International Conference on Intelligent Robots and Systems*. IEEE, 2012, pp. 1970–1975.

[4] P. M. Wensing, A. Wang, S. Seok, D. Otten, J. Lang, and S. Kim, "Proprioceptive actuator design in the mit cheetah: Impact mitigation and high-bandwidth physical interaction for dynamic legged robots," *IEEE Transactions on Robotics*, vol. 33, no. 3, pp. 509–522, 2017.

[5] G. Bledt, M. J. Powell, B. Katz, J. Di Carlo, P. M. Wensing, and S. Kim, "Mit cheetah 3: Design and control of a robust, dynamic quadruped robot," in *2018 IEEE/RSJ International Conference on Intelligent Robots and Systems (IROS)*. IEEE, 2018, pp. 2245–2252.

[6] S. Seok, A. Wang, M. Y. M. Chuah, D. J. Hyun, J. Lee, D. M. Otten, J. H. Lang, and S. Kim, "Design principles for energy-efficient legged locomotion and implementation on the mit cheetah robot," *Ieee/asme transactions on mechatronics*, vol. 20, no. 3, pp. 1117–1129, 2015.

[7] B. Katz, "A low cost modular actuator for dynamic robots," Master's thesis, Massachusetts Institute of Technology, 2018.

[8] Y. Ding and H.-W. Park, "Design and experimental implementation of a quasi-direct-drive leg for optimized jumping," in *2017 IEEE/RSJ International Conference on Intelligent Robots and Systems (IROS)*. IEEE, 2017, pp. 300–305.

[9] D. J. Blackman, J. V. Nicholson, C. Ordonez, B. D. Miller, and J. E. Clark, "Gait development on minitaur, a direct drive quadrupedal robot," in *Unmanned Systems Technology XVIII*, vol. 9837. International Society for Optics and Photonics, 2016, p. 98370I.

[10] T. Elery, S. Rezazadeh, C. Nesler, J. Doan, H. Zhu, and R. D. Gregg, "Design and benchtop validation of a powered knee-ankle prosthesis with high-torque, low-impedance actuators," in *2018 IEEE International Conference on Robotics and Automation (ICRA)*. IEEE, 2018, pp. 2788–2795.

[11] J. Tan, T. Zhang, E. Coumans, A. Iscen, Y. Bai, D. Hafner, S. Bohez, and V. Vanhoucke, "Sim-to-real: Learning agile locomotion for quadruped robots," *arXiv preprint arXiv:1804.10332*, 2018.

[12] I. W. Hunter, J. M. Hollerbach, and J. Ballantyne, "A comparative analysis of actuator technologies for robotics," *Robotics Review*, vol. 2, pp. 299–342, 1991.

[13] E. Sevinchan, I. Dincer, and H. Lang, "A review on thermal management methods for robots," *Applied Thermal Engineering*, 2018.

[14] A. Mazumdar, S. J. Spencer, C. G. Hobart, M. Kuehl, G. P. Brunson, N. M. Coleman, and S. Buerger, "Improving robotic actuator torque density and efficiency through enhanced heat transfer." Sandia National Lab.(SNL-NM), Albuquerque, NM (United States), Tech. Rep., 2016.

[15] J. Urata, T. Hirose, Y. Namiki, Y. Nakanishi, I. Mizuuchi, and M. Inaba, "Thermal control of electrical motors for high-power humanoid robots," in *2008 ieee/rsj international conference on intelligent robots and systems*. IEEE, 2008, pp. 2047–2052.

[16] J. Urata, Y. Nakanishi, K. Okada, and M. Inaba, "Design of high torque and high speed leg module for high power humanoid," in *2010 IEEE/RSJ International Conference on Intelligent Robots and Systems*. IEEE, 2010, pp. 4497–4502.

[17] N. Paine and L. Sentis, "Design and comparative analysis of a retrofitted liquid cooling system for high-power actuators," in *Actuators*, vol. 4, no. 3. Multidisciplinary Digital Publishing Institute, 2015, pp. 182–202.

[18] D. C. Hanselman, *Brushless Permanent-Magnet Motor Design*. Magna Physics Publishing, 2006.

[19] "Field orientated control of 3-phase ac-motors," 1998, https://www.ti.com/lit/an/bpra073/bpra073.pdf.

[20] "Um1052: Stm32 pmsm single/dual foc sdk v4.3," 2016, https://www.st.com/content/ccc/resource/technical/document/user_manual/5e/5e/d2/cb/07/35/45/a6/CD00298474.pdf/files/CD00298474.pdf/jcr:content/translations/en.CD00298474.pdf.

[21] M. Piccoli and M. Yim, "Cogging torque ripple minimization via position based characterization," in *Robotics: Science and Systems*, 2014.

[22] S. J. Jorgensen, J. Holley, F. Mathis, J. Mehling, and L. Sentis, "Thermal recovery of multi-limbed robots with electric actuators," *IEEE Robotics and Automation Letters*, 2019.

[23] J. Yu, J. Hooks, X. Zhang, M. S. Ahn, and D. Hong, "A proprioceptive, force-controlled, non-anthropomorphic biped for dynamic locomotion," in *2018 IEEE-RAS 18th International Conference on Humanoid Robots (Humanoids)*. IEEE, 2018, pp. 1–9.